

Dipole Anisotropy in Integrated Linearly Polarized Flux Density in NVSS Data

Prabhakar Tiwari and Pankaj Jain

Department of Physics, Indian Institute of Technology, Kanpur - 208016, India

13 September 2018

ABSTRACT

We study the dipole anisotropy in integrated linearly polarized flux density in NRAO VLA Sky Survey (NVSS). We extract the anisotropy parameters in the number counts, number counts weighted by polarization observables, i.e. polarized flux (P) and degree of polarization (p). We consider data with several different cuts on the flux density, $S > 10, 20, 30, 40, 50, 75$ mJy. For studies with polarized flux we impose the additional cut $0.5 < P < 100$ mJy. Similarly for degree of polarization we impose the cut, $0.01 < p < 1$. We find a very significant signal of dipole, both in number counts and P or p weighted number counts. The polar angle, θ , of the extracted dipole axis, for the case of number counts, shows a significant dependence on the flux density cut. This dependence indicates the presence of significant bias in the data. We find that the dipole parameters for the case of number counts weighted by polarized flux density are relatively stable. We argue that this parameter is relatively free of bias and study it in greater detail. The observed anisotropy is found to be much larger in comparison to the CMBR expectations. We find that polarization observables show a much higher level of anisotropy in comparison to pure number counts or sky brightness.

Key words: polarization, galaxies: high-redshift, galaxies: active

1 INTRODUCTION

There currently exists considerable evidence in favor of a large scale anisotropy in the Universe with the preferred axis pointing roughly in the direction of Virgo, close to the CMBR dipole. This includes, radio (Jain & Ralston 1999) and optical polarizations (Hutsemékers 1998; Hutsemékers & Lamy 2001; Jain et al. 2004), CMBR quadrupole and octopole (de Oliveira-Costa et al. 2004) as well as the radio source distribution and brightness (Blake & Wall 2002; Singal 2011; Gibelyou & Huterer 2012; Rubart & Schwarz 2013; Tiwari et al. 2013). The physical reason for these observations is not clear and points towards a violation of the cosmological principle. It might be possible to generate such an anisotropy even within the framework of the inflationary big bang cosmology. This is due to the modes which get produced during the anisotropic pre-inflationary phase of cosmic evolution (Aluri & Jain 2012).

A dipole anisotropy is expected in the radio source distribution as well as sky brightness due to Doppler and aberration effects which arise due to our local motion (Ellis & Baldwin 1984). CMBR observations indicate that our velocity relative to the cosmic rest frame is 369 ± 0.9 km/s in the direction, $l = 263.99^\circ \pm 0.14^\circ$, $b = 48.26 \pm 0.03^\circ$ in galactic coordinates (Kogut et al. 1993; Hinshaw et al. 2009). The direction parameters in J2000 equatorial system are $RA = 167.9^\circ$, $DEC = -6.93^\circ$. There have been many studies which attempt to extract the resulting dipole anisotropy in radio data (Baleisis et al. 1998; Blake & Wall 2002; Crawford 2009; Singal 2011; Gibelyou & Huterer 2012; Rubart & Schwarz 2013; Tiwari et al. 2013). Surprisingly, the observed anisotropy in radio data is found to be much larger (Singal 2011; Gibelyou & Huterer 2012; Rubart & Schwarz 2013; Tiwari et al. 2013) in comparison to prediction based on CMBR observations. However, the direction of the dipole agrees, within errors, with the CMBR direction. Observations also suggest that the amplitude of anisotropy in polarization observables (Jain & Ralston 1999) may be larger in comparison to number counts of radio sources or sky brightness (Singal 2011; Tiwari et al. 2013). We point out that diffuse x-ray background also indicates a dipole anisotropy (Boughn et al. 2002), whose direction and amplitude are found to be consistent with the CMBR dipole.

In the present paper we study the dipole anisotropy in radio polarization data using the NRAO VLA Sky Survey (NVSS) (Condon et al. 1998). We study the anisotropy in number counts after imposing a cut on the polarization flux (P) such that

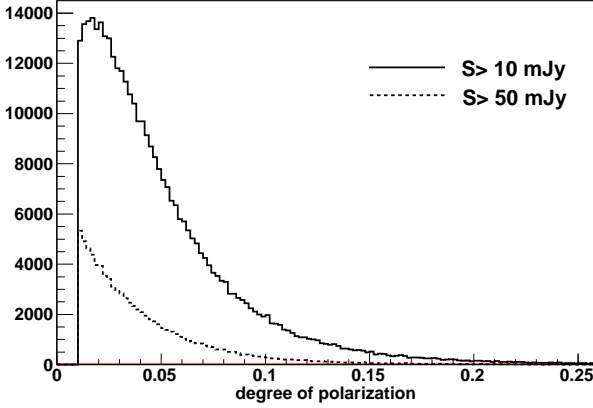


Figure 1. The distribution of degree of polarization for NVSS data after imposing cuts on the flux density, $S > 10$ mJy (solid line) and $S > 50$ mJy (dotted line). Here we have also imposed the cut, $p > 0.01$.

$0.5 \text{ mJy} < P < 100 \text{ mJy}$ and independently with a cut on degree of polarization (p), such that $0.01 < p < 1$. We also study the anisotropy in number counts weighted by these polarization observables. The polarization cuts are imposed to select only significantly polarized sources. An important concern in the present study is the possible presence of bias in number counts as a function of declination or the polar angle. Such a bias is known to exist in the case of number counts of full data, which includes both polarized and unpolarized sources (Blake & Wall 2002). This bias gets much reduced if we impose a cut on the flux density, S , of sources, such that, $S < 15$ mJy. This is indicated by the fact that the extracted dipole vector does not show a strong dependence on the lower limit on the flux density, as long as this limit is greater than 15 mJy (Tiwari et al. 2013). This declination dependent bias might be even larger in the case of polarized sources. We pay careful attention to this problem and identify an observable which is relatively stable to different cuts imposed on data. Our results suggest that the most reliable variable is the number counts weighted by polarization flux density. Hence we study it in considerable detail after imposing more stringent cuts on polarized flux and error in polarized flux.

We follow the procedure used by Tiwari et al. (2013) and extract the dipole by expanding the observables in spherical harmonics. The significance of dipole is calculated by comparing the dipole power of data with that of 10000 randomly generated isotropic samples. We consider several cuts $S > 10, 20, 30, 40, 50, 75$ mJy on flux density, S . Due to aberration and Doppler effects we expect that the number counts as well as the number counts weighted by P or p should display a dipole anisotropy. We determine the expected kinematic dipole and extract the local speed in these cases.

2 THE DATA

We use data from the NRAO VLA Sky Survey (NVSS) (Condon et al. 1998). It is a radio continuum survey at 1.4 GHz, covering the sky north of $\delta = -40^\circ$, where δ is the J2000 declination. The data product contains a catalogue of 1773484 radio sources. We follow Blake & Wall (2002) to impose different cuts on intensity. We remove Galactic contamination by masking the Galactic plane within latitude $|b| < 15^\circ$. Furthermore, we remove the clustering dipole (Blake & Wall 2002) by removing the sources within 30 arcsec of known nearby galaxies as listed in Saunders et al. (2000) and in third reference catalogue of bright Galaxies (RC3) (de Vaucouleurs et al. 1991; Corwin et al. 1994). In addition we also impose cuts on the polarization observables. The histogram of the degree of polarization is given in Fig. 1.

We use HEALPix¹ equal area pixelization scheme (Nside=16) to bin the sources in equal area pixels of $\sim 3.7^\circ$. The distribution of the number of significantly polarized sources per pixel is shown in Fig. 2. In this figure we have imposed the cuts, $S > 20$ mJy and $0.5 < P < 100$ mJy.

3 PROCEDURE

The polarized flux density, $P(\theta, \phi) = \sqrt{Q^2 + U^2}$ and degree of polarization, $p(\theta, \phi) = \sqrt{Q^2 + U^2}/S$, where Q and U are the standard Stokes parameters. Here (θ, ϕ) represent the spherical polar coordinates of the source. We use J2000 equatorial coordinate system, such that $RA = \phi$ and $Dec = 90 - \theta$. Both P and p are invariant under rotations about the direction of

¹ <http://healpix.jpl.nasa.gov/>

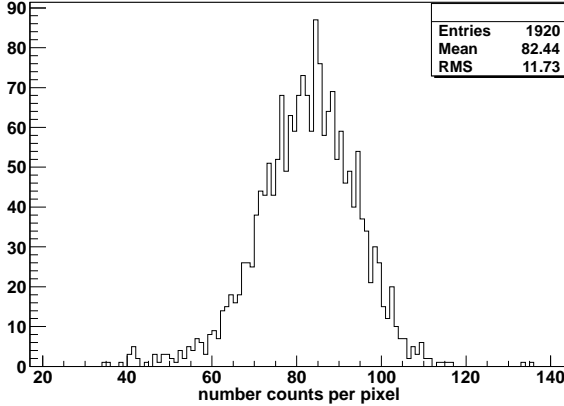


Figure 2. The distribution of number counts of significantly polarized sources for $N_{\text{side}}=16$. Here we have imposed the cuts, $S > 20$ mJy and $0.5 < P < 100$ mJy where S is the flux density and P the polarized flux density.

propagation. We rewrite these fields as $P(\theta, \phi) = P_0(1 + \Theta(\theta, \phi))$, with a similar equation for $p(\theta, \phi)$. Here $\Theta(\theta, \phi)$ represents the real space fluctuations of the polarization field. To study the correlations of this polarization field we expand it in spherical harmonics,

$$\Theta(\theta, \phi) = \sum_{l=1}^{\infty} \sum_{m=-l}^{+l} a_{lm} Y_{lm}(\theta, \phi), \quad (1)$$

where $Y_{lm}(\theta, \phi)$ are the usual spherical harmonics and a_{lm} the expansion parameters. The power for each multipole is given by,

$$C_l = \frac{1}{(2l+1)} \sum_{m=-l}^l |a_{lm}|^2. \quad (2)$$

A significant value of C_l indicates anisotropy at a scale $\sim (\pi/l)$ radian. In particular, C_1 represents the dipole term and its relation with dipole amplitude D is (Gibelyou & Huterer 2012),

$$C_1 = \frac{4\pi}{9} D^2. \quad (3)$$

Anisotropy in number counts is expected due to aberration and Doppler effects caused by local motion (Ellis & Baldwin 1984). Let ν_o and ν_r represent the observed and rest frame frequencies respectively. These are related by $\nu_o = \nu_r \delta$ where, $\delta = 1 + v \cos \theta / c$, where v is the local speed and θ the angle between the direction of observation and the local velocity. The polarized flux density and the degree of polarization (Eichendorf & Reinhardt 1979; Mesa et al. 2002; Tucci et al. 2004; Jackson et al. 2010) also show a dependence on frequency. We assume that the polarized flux density, P , can be modelled, approximately, as $P \propto \nu^{-\alpha_P}$. The parameter, α_P , is so far unknown for NVSS data. Here we assume that $\alpha_P = 0.75$, same as α for intensity (Blake & Wall 2002). This value may be revised in future once more data spectral polarization data becomes available. Small changes in this parameter have minor effect on our results and do not affect our conclusions.

Let S represent the total flux density of a source. Let $n(\theta, \phi, P, S)$ denote the differential number count per unit solid angle per unit polarized flux density (P) per unit total flux density (S). In the cosmological rest frame, assuming isotropy, we may model this as a power law in the parameters P and S , i.e.,

$$n_{rest}(\theta, \phi, P_{rest}, S_{rest}) \equiv \frac{d^3 N_{rest}}{d\Omega_{rest} dP_{rest} dS_{rest}} = k x x_P (P_{rest})^{-1-x_P} (S_{rest})^{-1-x} \quad (4)$$

where both P_{rest} and S_{rest} are in units of mJy. Here $d^3 N_{rest}$ represents the number of sources in a small bin, $d\Omega_{rest} dP_{rest} dS_{rest}$ in the rest frame. Here we have used a simple power behaviour assuming that S and P dependence may be decoupled from one another. These assumptions may not be exactly valid. The degree of polarization is also known to be anti-correlated with the flux density (Mesa et al. 2002; Tucci et al. 2004). Furthermore a simple power law may not provide a very good fit to data. However this model is reasonable to get an approximate estimate of the expected kinematic effect. More detailed fits, along the lines discussed in Tiwari et al. (2013), may be explored in future work. We obtain the values of x and x_P by fitting the data with different cuts. Let $d^3 N_{obs}$ represent the corresponding number of sources in the observer frame. We have (Ellis & Baldwin 1984; Tiwari et al. 2013),

$$d^3 N_{obs} = d^3 N_{rest} = n_{rest} d\Omega_{rest} dP_{rest} dS_{rest} = k x x_P (P_{obs})^{-1-x_P} (S_{obs})^{-1-x} \delta^{2+x(1+\alpha)+x_P(1+\alpha_P)} dP_{obs} dS_{obs} d\Omega_{obs} \quad (5)$$

where we have used $d\Omega_{obs} = d\Omega_{rest} \delta^{-2}$, $S \propto \nu^{-\alpha}$, $P \propto \nu^{-\alpha_P}$, $\nu_o = \nu_r \delta$, $S_{obs} = S_{rest} \delta^{1+\alpha}$, $P_{obs} = P_{rest} \delta^{1+\alpha_P}$.

The analysis above implies that we expect a dipole anisotropy in number counts of significantly polarized sources, given by,

$$D_N(v) = [2 + x(1 + \alpha) + x_P(1 + \alpha_P)](v/c). \quad (6)$$

We point out that here we have assumed that S and P are independent variables. The terms $x(1 + \alpha)$, $x_P(1 + \alpha_P)$ arise due to the lower limit imposed on S and P respectively. However we find that, for the case of real data, these two cuts are not independent. In particular a stringent cut on the flux density also eliminates most of the sources with low polarization and vice versa. Here we ignore this complication since the extracted velocity is not found to be physically relevant. As we shall see, the extracted dipole in all likelihood gets a large contribution from some unknown intrinsic effect.

We next consider the total polarized flux, P_I , i.e. the number counts weighted by the polarized flux density. This can be expressed as,

$$d^3 P_I = P d^3 N \quad (7)$$

In each pixel, this measure is computed by summing over the polarized flux density of all sources in the pixel. Following the procedure described above, we find that the expected dipole anisotropy, D_P , in this measure due to kinematic effects is identical to that expected in pure number counts, i.e.,

$$D_P(v) = [2 + x(1 + \alpha) + x_P(1 + \alpha_P)](v/c). \quad (8)$$

This is consistent with the result obtained earlier for unpolarized observables (Singal 2011; Tiwari et al. 2013), where it was found that the kinematic effects lead to identical dipole anisotropy in source counts and sky brightness if we assume a power law form of the differential number counts, $n(\theta, \phi, S)$.

We finally generalize this to the case of degree of polarization, $p = P/S$. The spectral dependence of p is given by, $p \propto \nu^{-\alpha_P + \alpha}$. We also define degree of polarization per unit frequency interval, p' . This is related to p by, $dp = p' d\nu$. We now repeat the above calculation using p' as the variable instead of P . We find that the dipole in number counts in this case is given by,

$$D_{N_p}(v) = [2 + x(1 + \alpha) + x_p(\alpha_p - 1)](v/c). \quad (9)$$

where $\alpha_p = \alpha_P - \alpha + 1$. We point out that in this case, $p'_{obs} = p'_{rest} \delta^{\alpha_p - 1}$. We also consider the dipole anisotropy in number counts weighted by the degree of polarization. This is defined by Eq. 7, with P replaced on the right hand side by p , i.e. $d^3 p_I = p d^3 N$. Our choice, $\alpha_P = \alpha$, implies that the degree of polarization is independent of frequency. This is in disagreement with the observations, which indicate an increase in p with frequency (Klein et al. 2003; Tucci et al. 2004). Hence it might be more reasonable to choose a smaller value of α_P . However, as discussed above, small changes in this parameter have negligible effect on our conclusions. In any case, a smaller value of α_P will further enhance the difference between the extracted local speed and that expected from CMBR observations. The amplitude of the dipole anisotropy in the number counts weighted by degree of polarization is also given by Eq. 9. The corresponding dipole anisotropy is denoted as D_p .

4 ANALYSIS METHOD AND BIAS SIMULATION

There are several regions of the sky for which data is not available. In particular we do not have data for $\delta < -40^\circ$ and we mask the Galactic plane within latitude $|b| < 15^\circ$ in order to remove the Galactic contamination. We create a full sky map by filling all of these empty pixels by randomly generated isotropic data (Tiwari et al. 2013). The random data is generated directly from the distribution observed for the real data set. For the number counts per pixel, this distribution is shown for a particular set of cuts in Fig. 2. The number of sources in empty pixels are obtained by randomly allocating the counts in filled pixels to the empty pixels. This preserves their distribution. Once the number count of sources in all the empty pixel is determined, the polarized flux of these sources is assigned by randomly extracting the values from real data. Hence the data in empty pixels has the same statistical properties as that in real pixels but does not have the large scale anisotropy, which might be present in real data. We make a spherical harmonic decomposition of the full sky map and extract the dipole parameters. The corresponding dipole power is denoted by C'_1 and the dipole axis parameters (θ', ϕ') , where θ' is the polar angle and ϕ' the RA. The extracted parameters would depend on the random sample used for filling the masked regions. Hence we repeat this process 1000 times. The final dipole parameters, C'_1 , θ' and ϕ' are obtained by taking the average over these 1000 realizations.

The random filling of empty pixels also adds a bias in dipole magnitude and direction. Hence the extracted average parameters C'_1 , θ' and ϕ' would contain some bias. We determine this bias by simulations. We generate full sky random samples which lead to a dipole anisotropy same as that seen in real data. We first generate an isotropic random map by randomly allocating NVSS data to different pixels. The procedure followed here is identical to that followed in filling the empty pixels in real data set, as described above. We then add a dipole with a magnitude and direction similar to that seen in real data. Let the input dipole power be denoted by C_1 , and the axes parameters, (θ, ϕ) . We next apply the same mask to the simulated maps as applied to real data. The pixels in the masked regions are filled by a procedure identical to that followed for

S_{low}	No. of Sources	k	$\Delta\theta$	$\Delta\phi$
Polarization flux density $0.5 < P < 100$ mJy				
10	236864	0.68 (0.14)	11.2 (12.6)	14.7 (15.7)
20	159533	0.72 (0.16)	4.3 (13.6)	13.0 (15.0)
30	118806	0.76 (0.20)	2.3 (16.1)	12.6 (17.8)
40	93425	0.75 (0.24)	-10.6 (22.5)	10.0 (26.0)
50	76205	0.71 (0.23)	-19.8 (23.6)	8.7 (28.8)
75	50576	0.70 (0.23)	-23.1 (24.5)	8.4 (34.8)
degree of polarization $0.01 < p < 1.0$				
10	280421	0.53 (0.09)	12.8 (9.6)	16.3 (13.3)
20	162350	0.65 (0.13)	10.5 (11.5)	13.9 (14.6)
30	110996	0.70 (0.16)	9.2 (13.8)	13.5 (15.9)
40	82457	0.75 (0.22)	-1.6 (19.8)	12.1 (21.7)
50	64611	0.77 (0.23)	-11.2 (19.5)	10.2 (23.8)
75	40300	0.77 (0.24)	-10.7 (19.5)	9.6 (24.7)

Table 1. The mean values of the bias factors k , $\Delta\theta$ and $\Delta\phi$ extracted from simulations corresponding to number counts of significantly polarized sources with a cut on polarization flux density ($0.5 < P < 100$ mJy) and degree of polarization ($0.01 < p < 1.0$). These values correspond to the bias generated in the dipole amplitude and direction due to the filling of masked sky with randomly generated data. The values in brackets are the standard deviations over 1000 samples.

S_{low}	No. of Sources	k	$\Delta\theta$	$\Delta\phi$
10	236864	0.70 (0.15)	-9.8 (12.6)	9.9 (12.5)
20	159533	0.67 (0.15)	-11.0 (14.0)	10.2 (14.3)
30	118806	0.68 (0.17)	-13.9 (15.7)	9.3 (17.3)
40	93425	0.63 (0.16)	-15.4 (16.2)	8.5 (19.7)
50	76205	0.62 (0.17)	-19.2 (17.8)	8.7 (21.7)
75	50576	0.65 (0.18)	-18.1 (18.7)	10.4 (22.5)

Table 2. The mean values of the bias factors, k , $\Delta\theta$ and $\Delta\phi$ extracted from simulations corresponding to number counts weighted by polarized flux density P using the cut, $0.5 < P < 100$ mJy. The values in brackets are the standard deviations over 1000 samples.

the real map. The difference between the dipole parameters extracted from the simulated map and the corresponding input parameters, gives a measure of the bias generated due to random filling of the masked sky. This procedure is iterated till the dipole parameters extracted from the simulated map match those of the real map. Hence the dipole parameters extracted from a simulated map are also equal to C'_1 , θ' and ϕ' , the same as those for real map. We have verified that the final result is independent of the initial guess used for the dipole vector. We generate 1000 random simulated maps. The output of each such map is equal to C'_1 , θ' and ϕ' , where as the input dipole parameters would differ due to the statistical fluctuations in the random realizations. The bias factor corresponding to the dipole power is defined as, $k^2 = C'_1/C_1$. Similarly the bias factors for angular variables are defined as, $\Delta\theta = \theta' - \theta$ and $\Delta\phi = \phi' - \phi$ (Tiwari et al. 2013).

We show the distributions of bias factors, k , $\Delta\phi$ and $\Delta\theta$, extracted from the 1000 simulated data sets, in Figs. 3 and 4. As the simulation is done for 1000 realizations, the error in the mean values of k , $\Delta\phi$ and $\Delta\theta$ is suppressed by a factor of $\sqrt{1000} \sim 31$, and negligible as compared to individual statistical error in dipole estimation. The extracted values of the bias factors are given in Tables 1-3. The real map dipole parameters are computed after correcting for this bias.

The significance of dipole is estimated by comparing the bias corrected power, C_1 , of the real data with the power, \tilde{C}_1 , of 10,000 full sky isotropic random realizations. These random samples are generated by using the same procedure employed for filling the empty pixels in real data, as described above. The significance is quoted in terms of the P-value, which is defined as the probability that an isotropic random sample may yield the dipole power larger than that observed in real data. We estimate it by counting the number of random samples which yield a higher power compared to real data. In case we find that none of the random power exceeds the real data, the P-value is less than 10^{-4} , which represents roughly a 4σ detection of the dipole anisotropy.

5 RESULTS

The distributions of C'_1 (real data) and \tilde{C}_1 (random isotropic data) for number counts of significantly polarized sources after imposing the cuts $0.5 < P < 100$ mJy and $S_{low} = 20$ mJy are shown in Fig. 5. The corresponding plots for number counts

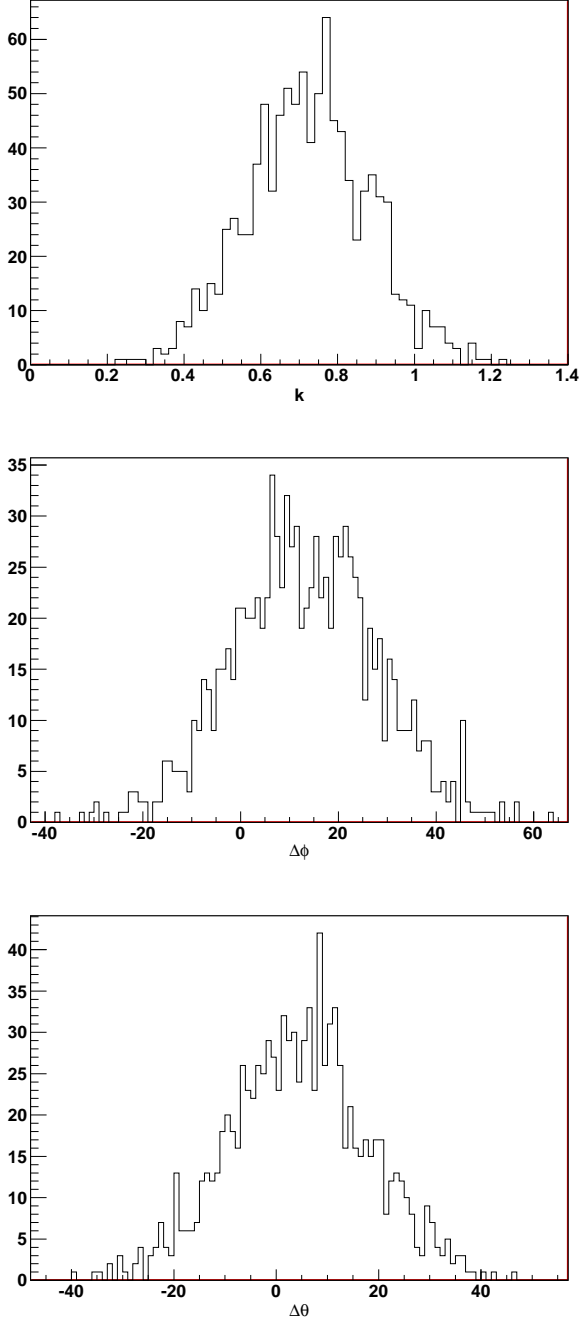


Figure 3. The distribution of the bias factors $k = \sqrt{C'_1/C_1}$, $\Delta\theta(\theta' - \theta)$ and $\Delta\phi(\phi' - \phi)$ for number counts of significantly polarized sources after imposing the cuts $S_{low} = 20$ mJy and $0.5 < P < 100$ mJy.

weighted by polarized flux density are shown in Fig. 6. The distribution of real data corresponds to random filling of the masked regions. The random map dipole power (\tilde{C}_1) is used to calculate the significance of dipole. The results for extracted dipole power, C'_1 , its significance and the direction parameters for number counts with a cut on polarized flux density, $0.5 < P < 100$ mJy, are given in Table 4 for different values of the lower limit on the flux density, $S_{low} = 10, 20, 30, 40, 50$ and 75 mJy. The results with a cut on degree of polarization, $0.01 < p < 1$, are also shown. The results for number counts weighted by polarized flux are given in Table 5. The corresponding results for degree of polarization are given in Table 6. The power corresponding to random isotropic samples is also shown. The data indicates a very significant signal of dipole anisotropy. In most cases the significance is 4σ or higher. The significance increases as we reduce the limiting value S_{low} . This arises mainly because of the

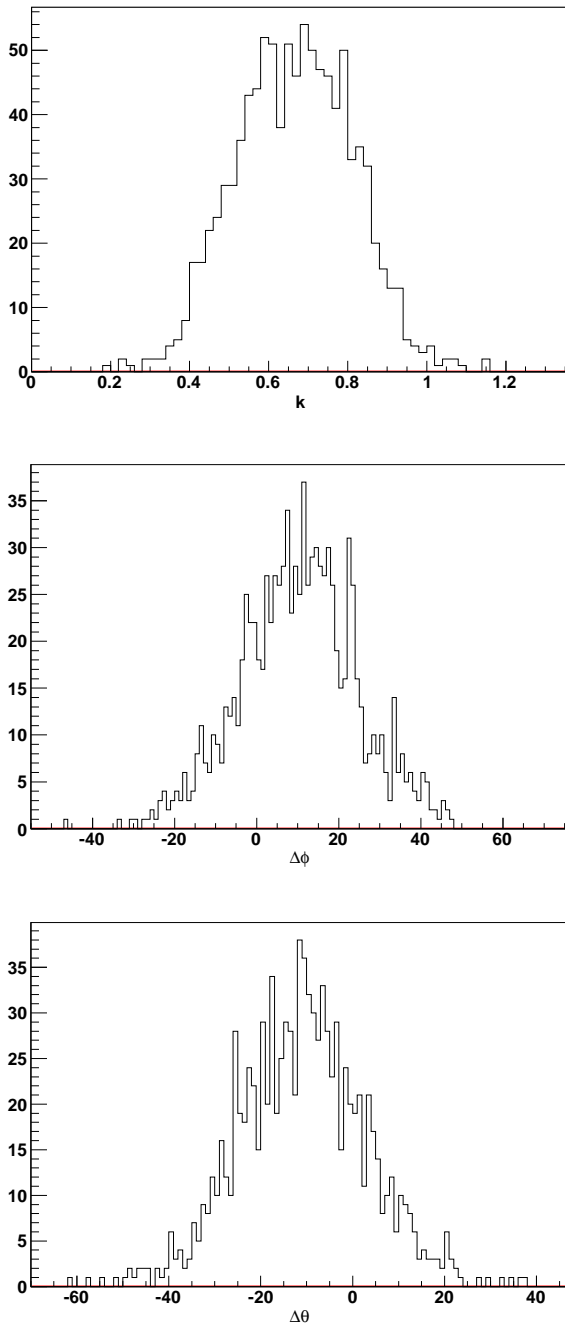


Figure 4. The distribution of the bias factors, $k = \sqrt{C'_1/C_1}$, $\Delta\theta(\theta' - \theta)$ and $\Delta\phi(\phi' - \phi)$ for number counts weighted by polarized flux after imposing the cuts $S_{low} = 20$ mJy and $0.5 < P < 100$ mJy.

increase in the number of sources as we reduce S_{low} , which leads to a decrease in the dipole power, \tilde{C}_1 , of isotropic random samples.

The bias corrected dipole amplitude and direction parameters for number counts, D_N and D_{Np} , are given in Tables 7 and 8 respectively. The results for number counts weighted polarized flux density are given in Table 9. The corresponding results for degree of polarization are in Table 10. If we assume that the dipole arises primarily due to our local motion, the speed turns out to be much larger in comparison to the CMBR expectations. The exponents x for the power law fit to the number density $n(S, P)$ are found to be, $x = 0.759, 0.885, 0.959, 1.02, 1.06, 1.25$ for the cuts $S_{low} = 10, 20, 30, 40, 50$ and 75 mJy respectively. This is obtained by imposing no cut on P . The exponent x_P is determined from the data after imposing the cut $0.5 < P < 100$ mJy and no cut on S . We obtain $x_P = 1.2$. As discussed in section 3, we set $\alpha_P = 0.75$. The extracted speed

S_{low}	No. of Sources	k	$\Delta\theta$	$\Delta\phi$
10	280421	0.67 (0.10)	8.0 (8.2)	13.8 (9.3)
20	162350	0.66 (0.11)	-0.6 (9.0)	11.0 (9.5)
30	110996	0.67 (0.14)	-5.0 (11.9)	10.1 (12.4)
40	82457	0.61 (0.14)	-13.4 (14.1)	6.8 (15.6)
50	64611	0.57 (0.14)	-17.1 (14.3)	9.2 (17.6)
75	40300	0.58 (0.15)	-19.2 (15.6)	5.7 (19.6)

Table 3. The mean values of the bias factors, k , $\Delta\theta$ and $\Delta\phi$ extracted from simulations corresponding to number counts weighted by degree of polarization p ($0.01 < p < 1.0$). The values in brackets are the standard deviations over 1000 samples.

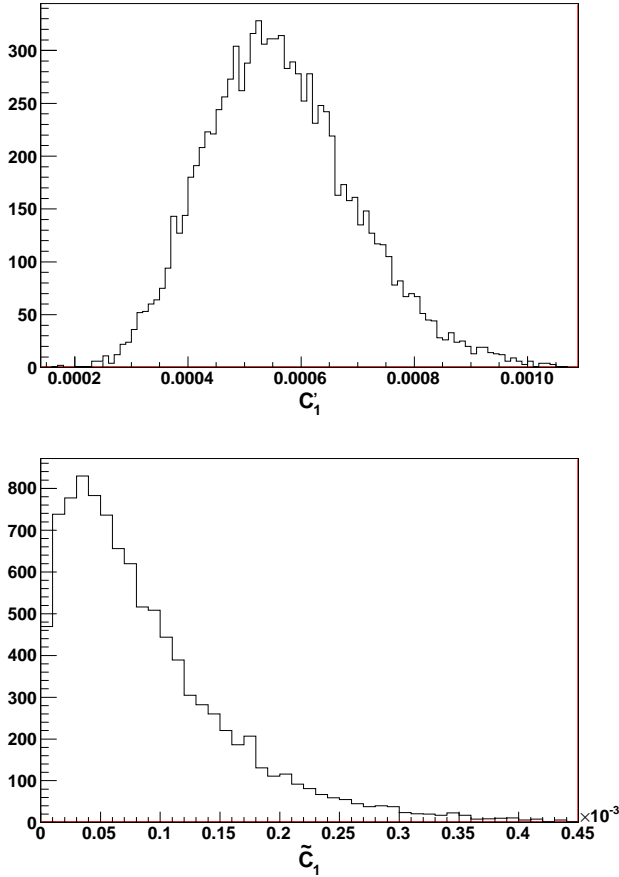


Figure 5. The distribution of dipole power for number counts of significantly polarized sources for the case of real data (upper graph) and isotropic random simulated data (lower graph). Here we have imposed the cuts $S_{low} = 20$ mJy and $0.5 < P < 100$ mJy. The distribution in real data is obtained by randomly filling in the masked regions, as explained in text.

for the case of number counts weighted by polarized flux density is given in Table 11. Here the speed is extracted assuming that the dipole arises entirely due to kinematic effects. We find that the extracted dipole cannot be consistently attributed to kinematic effects, predicted on the basis of CMBR dipole. The speed turns out to be about 6-7 times larger. Similar results are obtained with number counts. For comparison, the extracted dipole from number counts as well as sky brightness, without considering polarization properties of the radio sources, is found to be about 3-4 times larger than that predicted by CMBR (Tiwari et al. 2013). This indicates the presence of a larger intrinsic dipole in the polarized sample. Hence we speculate that the physical mechanism responsible for the intrinsic dipole affects the polarization more than the flux.

We find that the polar angle, θ , of the dipole axis shows a strong dependence on S_{low} for several cases. In contrast, the dipole amplitude as well as the azimuthal angle are found to be relatively stable. The dependence on S_{low} can only be attributed to the presence of θ dependent bias in the number counts of significantly polarized sources. Such a bias is also present in the complete data set, which includes both unpolarized and polarized sources (Blake & Wall 2002). In this case

S_{low}	$C'_1 (\times 10^3)$	$\tilde{C}_1 (\times 10^3)$	P-value	$\theta'(^{\circ})$	$\phi'(^{\circ})$
polarized flux density $0.5 < P < 100$ mJy					
10	0.496 ± 0.114	0.072 ± 0.059	$< 10^{-4}$	63 ± 9	151 ± 8
20	0.565 ± 0.133	0.090 ± 0.074	$< 10^{-4}$	74 ± 10	150 ± 8
30	0.488 ± 0.132	0.109 ± 0.089	$< 10^{-3}$	77 ± 12	152 ± 9
40	0.351 ± 0.135	0.134 ± 0.110	2.3×10^{-3}	95 ± 15	147 ± 12
50	0.440 ± 0.165	0.161 ± 0.132	9×10^{-4}	106 ± 14	159 ± 13
75	0.577 ± 0.227	0.220 ± 0.182	1.6×10^{-3}	109 ± 14	162 ± 14
degree of polarization $0.01 < p < 1$					
10	0.77 ± 0.16	0.062 ± 0.050	$< 10^{-4}$	49 ± 7	136 ± 6
20	0.68 ± 0.15	0.086 ± 0.071	$< 10^{-4}$	65 ± 9	146 ± 7
30	0.67 ± 0.16	0.114 ± 0.093	$< 10^{-4}$	69 ± 10	150 ± 8
40	0.51 ± 0.17	0.151 ± 0.123	7×10^{-4}	84 ± 14	146 ± 10
50	0.62 ± 0.20	0.188 ± 0.154	8×10^{-4}	95 ± 13	158 ± 11
75	0.87 ± 0.29	0.279 ± 0.231	10×10^{-3}	95 ± 14	157 ± 12

Table 4. The extracted value of the dipole power C'_1 and the corresponding value for simulated random data \tilde{C}_1 using number counts for different cuts on flux density of a source ($S > S_{low}$) along with cut on polarized flux density $0.5 \text{ mJy} < P < 100 \text{ mJy}$ or degree of polarization, $0.01 < p < 1$. The significance of the dipole anisotropy is given in terms of the P-value. The extracted parameters of the dipole axis, θ' and ϕ' are also shown.

S_{low}	$C'_1 (\times 10^3)$	$\tilde{C}_1 (\times 10^3)$	P-value	$\theta'(^{\circ})$	$\phi'(^{\circ})$
10	1.36 ± 0.41	0.17 ± 0.14	$< 10^{-4}$	95 ± 12	153 ± 10
20	1.45 ± 0.48	0.21 ± 0.17	$< 10^{-4}$	99 ± 13	151 ± 11
30	1.39 ± 0.50	0.26 ± 0.21	$< 10^{-4}$	103 ± 14	152 ± 12
40	1.41 ± 0.55	0.30 ± 0.25	$< 10^{-4}$	108 ± 14	152 ± 13
50	1.55 ± 0.60	0.35 ± 0.29	$< 10^{-4}$	111 ± 14	159 ± 14
75	1.80 ± 0.71	0.46 ± 0.38	$< 10^{-4}$	110 ± 15	162 ± 14

Table 5. The extracted value of the dipole power C'_1 and the corresponding value for simulated isotropic data \tilde{C}_1 using number count weighted by polarized flux density P ($0.5 < P < 100$) for different cuts on flux density of a source ($S > S_{low}$). The significance of the dipole anisotropy, P-value, as well as the extracted dipole axis parameters, θ' and ϕ' are also shown.

it practically gets eliminated in data with $S > 15$ mJy. However in the present case the bias seems to be present for larger values of the lower limit on the flux density. We notice that the parameters for the case of polarized flux weighted number counts, Table 9, are relatively stable with the cut on flux density, S . This trend is understandable since, in this case, the contribution due to the data with low flux is reduced. This reduces the systematic effects that might be present due to faint sources. Similar trend was seen for the case of flux density weighted number counts (Tiwari et al. 2013). Hence the results for the case of number counts weighted by polarization flux density may be relatively free of bias. For this reason we study this observable in considerable detail.

S_{low}	$C'_1 (\times 10^3)$	$\tilde{C}_1 (\times 10^3)$	P-value	$\theta'(^{\circ})$	$\phi'(^{\circ})$
10	1.32 ± 0.31	0.078 ± 0.064	$< 10^{-4}$	70 ± 10	149 ± 8
20	1.57 ± 0.44	0.12 ± 0.09	$< 10^{-4}$	83 ± 11	141 ± 8
30	1.26 ± 0.42	0.16 ± 0.13	$< 10^{-4}$	89 ± 13	142 ± 10
40	1.18 ± 0.47	0.21 ± 0.17	$< 10^{-4}$	103 ± 14	139 ± 11
50	1.37 ± 0.54	0.26 ± 0.21	$< 10^{-4}$	115 ± 13	154 ± 13
75	1.76 ± 0.68	0.38 ± 0.31	$< 10^{-4}$	116 ± 13	160 ± 14

Table 6. The extracted value of the dipole power C'_1 and the corresponding value for simulated isotropic data \tilde{C}_1 using number counts weighted by the degree of polarization p ($0.01 < P < 1$) for different cuts on flux density of a source ($S > S_{low}$). The significance of the dipole anisotropy, P-value, as well as the extracted dipole axis parameters, θ' and ϕ' , are also shown.

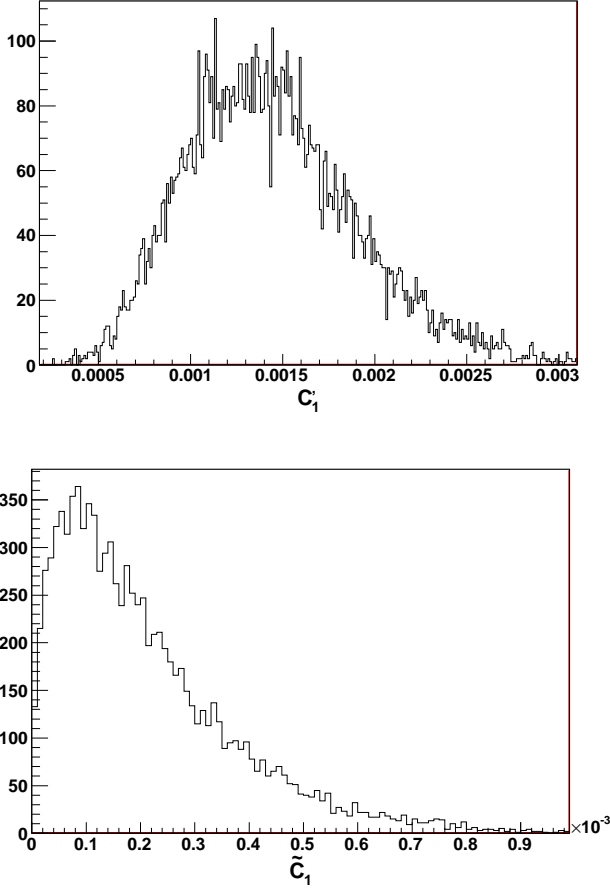


Figure 6. The distribution of dipole power for number counts weighted by polarized flux for the case of real data (upper graph) and isotropic random simulated data (lower graph). Here we have imposed the cuts $S_{low} = 20$ mJy and $0.5 < P < 100$ mJy. The distribution in real data is obtained by randomly filling in the masked regions, as explained in text.

S_{low}	D_N	$\theta(^{\circ})$	$\phi(^{\circ})$
10	0.028 ± 0.003	51 ± 9	137 ± 8
20	0.028 ± 0.003	70 ± 10	137 ± 8
30	0.025 ± 0.003	75 ± 12	140 ± 9
40	0.021 ± 0.004	106 ± 15	137 ± 12
50	0.025 ± 0.005	126 ± 14	151 ± 13
75	0.029 ± 0.006	132 ± 14	154 ± 14

Table 7. The extracted dipole amplitude for number counts, D_N , and the corresponding direction parameters (θ , ϕ) for various cuts on the flux density for the cut on polarized flux, $0.5 < P < 100$ mJy.

S_{low}	D_{Np}	$\theta(^{\circ})$	$\phi(^{\circ})$
10	0.044 ± 0.005	36 ± 7	120 ± 6
20	0.034 ± 0.004	55 ± 9	132 ± 7
30	0.031 ± 0.004	60 ± 10	136 ± 8
40	0.026 ± 0.004	86 ± 14	134 ± 10
50	0.027 ± 0.004	106 ± 13	148 ± 11
75	0.033 ± 0.005	106 ± 14	147 ± 12

Table 8. The extracted dipole amplitude for number counts, D_{Np} , and the corresponding direction parameters (θ , ϕ) for various cuts on the flux density for the cut on degree of polarization, $0.01 < p < 1.0$.

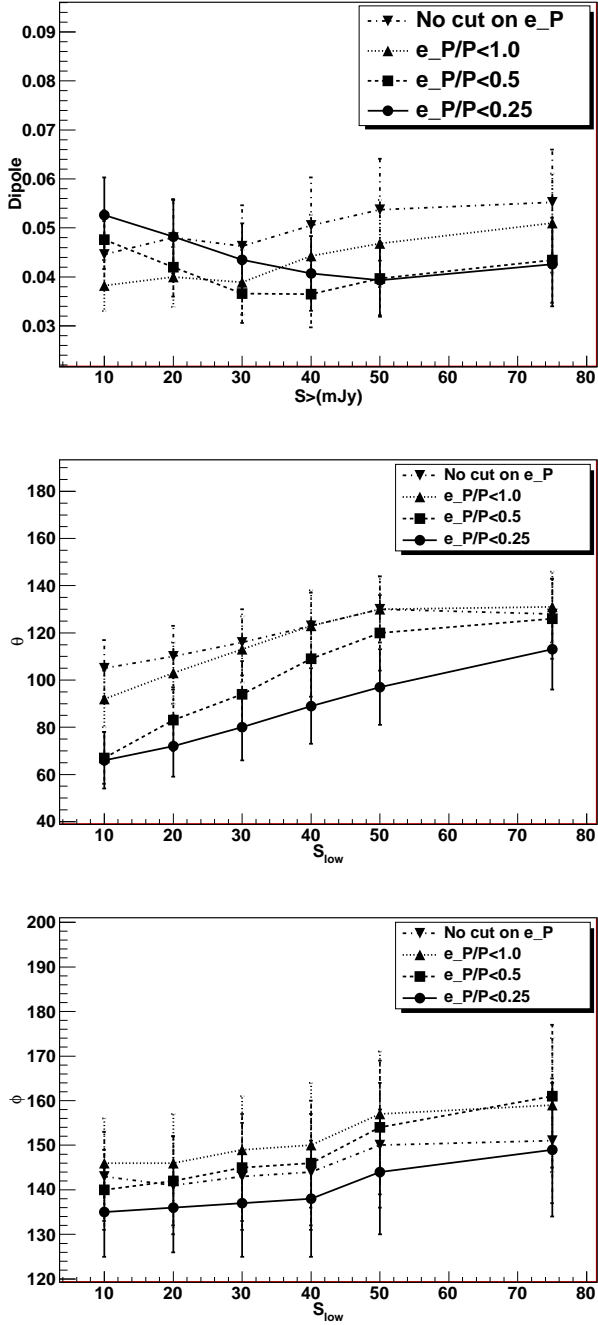


Figure 7. The dipole amplitude (upper graph), polar angle, θ , (middle graph) and ϕ or RA (lower graph) for number counts weighted by polarized flux as a function of lower limit on the flux density, S_{low} for different cuts on the fractional error in the polarized flux, $e_P/P < 1, 0.5, 0.25$. Here we have used the additional cut $0.5 < P < 100$ mJy.

5.1 The super-galactic plane

In our analysis we have eliminated sources which are likely to belong to the local supercluster using the catalogues of nearby galaxies (Saunders et al. 2000; de Vaucouleurs et al. 1991; Corwin et al. 1994). Here we follow an alternate procedure to eliminate the bias due to such sources. Their density is largest near the supergalactic plane. Hence we can determine their influence by masking this plane. Here we eliminate the region lying within $\pm 10^\circ$ of the supergalactic plane, besides imposing other cuts, described earlier. Here we study only the dipole amplitude, D_P , corresponding to the number counts weighted by polarized flux density. As we have argued above, this observable appears to be relatively free of bias. The extracted values of bias corrected dipole amplitude and direction parameters are given in Table 12. We find that the amplitude does not change

S_{low}	D_P	$\theta(^{\circ})$	$\phi(^{\circ})$
10	0.045 ± 0.007	105 ± 12	143 ± 10
20	0.048 ± 0.008	110 ± 13	141 ± 11
30	0.046 ± 0.008	116 ± 14	143 ± 12
40	0.051 ± 0.010	123 ± 14	144 ± 13
50	0.054 ± 0.010	130 ± 14	150 ± 14
75	0.055 ± 0.011	128 ± 15	151 ± 14

Table 9. The extracted dipole amplitude, D_P , for number counts weighted by the polarized flux density and the corresponding direction parameters (θ , ϕ) as a function of S_{low} for the polarized flux density lying in the range $0.5 < P < 100$ mJy.

S_{low}	D_p	$\theta(^{\circ})$	$\phi(^{\circ})$
10	0.046 ± 0.005	62 ± 10	135 ± 8
20	0.051 ± 0.007	84 ± 11	130 ± 8
30	0.045 ± 0.008	94 ± 13	132 ± 10
40	0.048 ± 0.010	117 ± 14	132 ± 11
50	0.055 ± 0.011	132 ± 13	144 ± 13
75	0.061 ± 0.012	136 ± 13	154 ± 14

Table 10. The extracted dipole amplitude, D_p , for the number counts weighted by the degree of polarization and the corresponding direction parameters (θ , ϕ) for various cuts on the flux density. Here we have imposed the cut on degree of polarization such that, $0.01 < p < 1$.

much with the super-galactic cut. Hence we conclude that the dipole anisotropy does not get significant contribution due to the local clustering effect. It is most likely a cosmological effect. The largest change for polarized flux weighted number counts is seen in the ϕ (or RA). However in this case also the results with and without the supergalactic cut agree within errors.

5.2 Polarized flux weighted number counts

In this section we study the dipole anisotropy, D_P , in number counts weighted by polarized flux density, P_I , in more detail by imposing further cuts to improve the quality of data. This observable is equal to the total polarized flux density in any pixel. As discussed above, we expect it to be more stable in comparison to pure number counts, which are dominated by low flux sources. We study the dipole anisotropy, D_P , by imposing further cuts on the fractional error in polarized flux, (e_P/P). We find that many sources, especially those with low polarized flux, have large error. Here we study how our results change as we impose the cuts, $e_P/P < 1$, 0.5 and 0.25. Furthermore we also determine the results with a more stringent cut on the polarized flux, $1 < P < 100$ mJy.

In Tables 13 and 14 we show the extracted dipole for a different cuts on the error in the polarized flux with a lower limit on the polarized flux equal to 0.5 mJy and 1.0 mJy respectively. We see that after imposing a cut on the error in polarized flux density, $e_P/P < 1$, the dipole amplitude becomes smaller in comparison to the case with no cut. However as we impose more stringent cuts, the amplitude shows relatively small change. One still observes some dependence on the lower limit of the flux density S_{low} . However this tends to saturate as we go to larger values of S_{low} . In Fig. 7, we plot the dipole amplitude and the direction parameters, (θ , ϕ), as a function of the lower limit, S_{low} , on the flux density. We find that the extracted values of the dipole power and ϕ agree with one another within errors for different cuts. The values of θ show a mild increase with S_{low} which tends to saturate for large values of S_{low} . In Fig. 7, such a saturation is not observed for the cut $e_P/P < 0.25$. However for this case also the extracted value of θ becomes uniform as we increase S_{low} to values larger than 75 mJy. Hence we do not observe a very strong dependence of any of these extracted parameters to the different cuts imposed.

Finally we determine how our results are affected by the bright and extended radio sources. Some of these sources would be misidentified as a cluster of very large number of sources in the NVSS survey (Blake & Wall 2002). Hence these are likely to introduce bias in our analysis. Blake & Wall (2002) identify 22 such regions. Tiwari et al. (2013) show that after imposing

S_{low}	10	20	30	40	50	75
v (Km/s)	2490 ± 390	2550 ± 420	2390 ± 420	2600 ± 510	2720 ± 500	2620 ± 520

Table 11. The extracted local speed for number counts weighted by polarized flux density, with the cut $0.5 < P < 100$ mJy.

S_{low}	D_P	$\theta(^{\circ})$	$\phi(^{\circ})$
10	0.044 ± 0.010	112 ± 17	139 ± 15
20	0.048 ± 0.011	118 ± 18	136 ± 16
30	0.048 ± 0.012	121 ± 19	138 ± 17
40	0.051 ± 0.013	131 ± 20	139 ± 19
50	0.054 ± 0.014	135 ± 20	146 ± 21
75	0.054 ± 0.015	133 ± 22	150 ± 22

Table 12. The extracted dipole amplitude D_P and the corresponding direction parameters (θ , ϕ) for various cuts on the flux density S and super galactic plane ($|b| > 10^{\circ}$). Here the polarized flux is confined to lie in the range $0.5 < P < 100$ mJy.

S_{low}	D_P	$\theta(^{\circ})$	$\phi(^{\circ})$
$e_P/P < 1$			
10	0.038 ± 0.005	92 ± 12	146 ± 10
20	0.040 ± 0.006	103 ± 13	146 ± 11
30	0.039 ± 0.007	113 ± 14	149 ± 12
40	0.044 ± 0.008	123 ± 15	150 ± 14
50	0.047 ± 0.009	130 ± 14	157 ± 14
75	0.051 ± 0.010	131 ± 15	159 ± 15
$e_P/P < 0.5$			
10	0.048 ± 0.006	67 ± 11	140 ± 9
20	0.042 ± 0.006	83 ± 13	142 ± 10
30	0.037 ± 0.006	94 ± 14	145 ± 12
40	0.037 ± 0.007	109 ± 16	146 ± 14
50	0.040 ± 0.008	120 ± 16	154 ± 15
75	0.043 ± 0.009	126 ± 17	161 ± 16
$e_P/P < 0.25$			
10	0.053 ± 0.008	66 ± 12	135 ± 10
20	0.048 ± 0.008	72 ± 13	136 ± 10
30	0.044 ± 0.007	80 ± 14	137 ± 12
40	0.041 ± 0.008	89 ± 16	138 ± 13
50	0.040 ± 0.007	97 ± 16	144 ± 14
75	0.043 ± 0.009	113 ± 17	149 ± 15

Table 13. The extracted dipole amplitude D_P and the corresponding direction parameters (θ , ϕ) for various cuts on the flux density and the fractional error on the polarized flux. Here the polarized flux density lies in the range $0.5 - 100$ mJy.

a cut which removes such sources, the extracted dipole amplitude gets reduced by about 10 – 20 %. In the present case of significantly polarized sources, however, we find that the contribution of these sources is much smaller. After imposing this cut, we find that the dipole amplitude changes by less than 10%. The direction parameters are found to be even less sensitive. Hence we conclude that these sources do not significantly affect our results.

6 DISCUSSION AND CONCLUSION

In this paper we have studied the dipole anisotropy in the number counts of radio sources after imposing cuts on the polarized flux density and independently on the degree of polarization. We have also studied the anisotropy in the number counts weighted by polarized flux and by degree of polarization. This study is important in view of the recently reported dipole anisotropy in radio source distribution (Blake & Wall 2002; Singal 2011; Gibelyou & Huterer 2012; Rubart & Schwarz 2013; Tiwari et al. 2013). Most of these studies find a dipole amplitude much larger than that predicted on the basis of CMBR dipole. We find that the dipole amplitude gets further enhanced after imposing cuts on polarized flux and the degree of polarization. The amplitude is found to be more than twice as large as that observed in the case unpolarized observables. The direction of the dipole is again found to be relatively close to the CMBR dipole. The dipole parameters, however, are found to show considerable dependence on the lower limit, S_{low} , imposed on the flux density. In particular the extracted value of

S_{low}	D_P	$\theta(^{\circ})$	$\phi(^{\circ})$
$e_P/P < 1$			
10	0.042 ± 0.006	98 ± 12	150 ± 10
20	0.042 ± 0.006	105 ± 13	146 ± 11
30	0.042 ± 0.007	114 ± 14	151 ± 12
40	0.044 ± 0.008	123 ± 15	150 ± 14
50	0.047 ± 0.009	129 ± 15	159 ± 14
75	0.049 ± 0.010	129 ± 15	160 ± 15
$e_P/P < 0.5$			
10	0.042 ± 0.005	82 ± 12	145 ± 10
20	0.040 ± 0.006	93 ± 13	146 ± 11
30	0.037 ± 0.006	104 ± 15	149 ± 12
40	0.040 ± 0.007	116 ± 16	149 ± 14
50	0.042 ± 0.008	125 ± 16	157 ± 15
75	0.044 ± 0.009	125 ± 16	161 ± 16
$e_P/P < 0.25$			
10	0.053 ± 0.008	66 ± 12	135 ± 10
20	0.048 ± 0.008	71 ± 13	136 ± 10
30	0.044 ± 0.007	79 ± 14	137 ± 12
40	0.041 ± 0.008	88 ± 16	138 ± 13
50	0.039 ± 0.007	97 ± 16	144 ± 14
75	0.043 ± 0.009	113 ± 17	149 ± 15

Table 14. The extracted dipole amplitude D_P and the corresponding direction parameters (θ , ϕ) for various cuts on the flux density and the fractional error on polarized flux. Here the polarized flux density lies in the range 1.0 – 100 mJy.

the polar angle θ is found to show rather large variation with S_{low} for the case of number counts as well as number counts weighted by degree of polarization. This variation can be attributed to the presence of θ dependent bias in data.

The variation in θ in the case of number counts weighted by polarized flux density, however, is found to be relatively small. This motivates us to study this observable in greater detail. This observable is also physically relevant since it represents the total polarized flux in each pixel. We study the dipole anisotropy in this observable for several different different cuts which eliminates data with large error in polarized flux density. We also determine the change in signal with increase in the lower limit on the polarized flux density. We find that the dipole amplitude in this case is relatively stable with these changes. The results for different cuts agree within errors. The extracted azimuthal angle of the dipole axis is also found to be stable. The maximum change is seen in the polar angle, θ . However in this case also the result stabilizes as we go to larger values of S_{low} .

The observed anisotropy cannot be attributed to the local supercluster. In our study we remove sources lying in our local neighbourhood. These sources are identified by using the catalogues provided in (Saunders et al. 2000; de Vaucouleurs et al. 1991; Corwin et al. 1994). Alternatively we have also studied the signal after eliminating the supergalactic plane. The results do not depend very strongly on these cuts.

Finally, we calculate the velocity for the case of number counts weighted by polarized flux density. Here we assume that the polarized flux follows a power law dependence on frequency ($P \propto \nu^{-\alpha_P}$), similar to intensity. The extracted speed turns out to be even larger in comparison to that extracted without imposing polarization cuts (Singal 2011; Tiwari et al. 2013). In this analysis we assume that $\alpha_P \approx \alpha$, the flux spectral index. This value may be subject to change once better polarization spectral data becomes available.

We conclude that the anisotropy in polarization observables is much stronger in comparison to flux observables. This is consistent with the earlier claim of significant dipole anisotropy in the polarization offset angle (Jain & Ralston 1999).

There now exist many independent observations which indicate a preferred direction pointing roughly towards Virgo. It is unlikely that all of them can be explained by some systematic effect. For example, the NVSS data is more likely to pick a preferred axis pointing towards the poles due to systematic effect arising due to sources with low flux (Blake & Wall 2002). The direction observed, however, is nearly perpendicular to that. The dependence of direction with the cut on flux density might be explained by this systematic effect. This dependence is most prominent in number counts but is relatively small in the flux weighted number counts (Tiwari et al. 2013) as well as polarized flux weighted number counts. Furthermore it seems very unlikely that systematic effects would pick the same direction in so many different observations, i.e. radio polarizations orientations (Jain & Ralston 1999), optical polarizations (Hutsemékers 1998), CMBR quadrupole and octopole (de Oliveira-Costa et al. 2004), radio number counts (Blake & Wall 2002; Singal 2011) and radio polarized flux (present work). In all likelihood this alignment of axes (Ralston & Jain 2004; Schwarz et al. 2004) is caused by a physical effect. There exist

many models which might explain the observed large scale anisotropy. An interesting possibility, within the framework of the Big Bang model, is that the modes generated during the pre-inflationary anisotropic expansion might enter the horizon at late times and cause to observe large scale anisotropy (Aluri & Jain 2012; Rath et al. 2013). The early phase of expansion is expected to be anisotropic, which evolves into an isotropic Universe during inflation (Wald 1983). The large scale anisotropy may also affect the intergalactic magnetic field which may influence the source magnetic field and hence its polarized radiation. A detailed investigation of the physical mechanism is postponed to future work.

ACKNOWLEDGEMENTS

We have used CERN ROOT 5.27 for generating our plots. Some of the results in this paper have been derived using the HEALPix (Gořski et al. 2005) package. Prabhakar Tiwari sincerely acknowledge CSIR, New Delhi for award of fellowship during the work. We thank William Cotton for useful comments on the paper.

REFERENCES

- Aluri P. K., Jain P., 2012, *Mod. Phys. Lett. A*, 27, 1250014
Baleisis A., Lahav O., Loan A. J., Wall J. V., 1998, *MNRAS*, 297, 545
Blake C., Wall J., 2002, *Nature*, 416, 150
Boughn S. P., Crittenden R. G., Koehrsen G. P., 2002, *ApJ*, 580, 672
Condon J. J., Cotton W. D., Greisen E. W., Yin Q. F., Perley R. A., Taylor G. B., Broderick J. J., 1998, *AJ*, 115, 1693
Corwin Jr. H., Buta R., de Vaucouleurs G., 1994, *AJ*, 108, 2128
Crawford F., 2009, *ApJ*, 692, 887
de Oliveira-Costa A., Tegmark M., Zaldarriaga M., Hamilton A., 2004, *Phys. Rev. D*, 69, 063516
de Vaucouleurs G., de Vaucouleurs A., Corwin H. G., Buta R. J., Paturel G., Fouque P., 1991, *Third Reference Catalogue of Bright Galaxies (RC3)*. Springer-Verlag, New York
Eichendorf W., Reinhardt M., 1979, *Ap&SS*, 61, 153
Ellis G. F. R., Baldwin J. E., 1984, *MNRAS*, 206, 377
Gibelyou C., Huterer D., 2012, *MNRAS*, 427, 1994
Gořski K., Hivon E., Banday A., Wandelt B., Hansen F., et al., 2005, *ApJ*, 622, 759
Hinshaw G., Weiland J. L., Hill R. S., Odegard N., Larson C., et al., 2009, *ApJS*, 180, 225
Hutsemékers D., 1998, *A&A*, 332, 410
Hutsemékers D., Lamy H., 2001, *A&A*, 367, 381
Jackson N., Browne I. W. A., Battye R. A., Gabuzda D., Taylor A. C., 2010, *MNRAS*, 401
Jain P., Narain G., Sarala S., 2004, *MNRAS*, 347, 394
Jain P., Ralston J. P., 1999, *Mod. Phys. Lett. A*, 14, 417
Klein U., Mack K.-H., Gregorini K.-H., Vigotti M., 2003, *A&A*, 406, 579
Kogut A., Lineweaver C., Smoot G. F., Bennett C. L., Banday A., et al., 1993, *ApJ*, 419, 1
Mesa D., Baccigalupi C., De Zotti G., Gregorini K.-H., Vigotti M., Klein U., 2002, *Astronomy & Astrophysics*, 396
Ralston J. P., Jain P., 2004, *Int. J. Mod. Phys. D*, 13, 1857
Rath P., Mudholkar T., Jain P., Aluri P., Panda S., 2013, *Journal of Cosmology and Astroparticle Physics*, 4, 7
Rubart M., Schwarz D. J., 2013, *A&A*, 555
Saunders W., Sutherland W., Maddox S., Keeble O., Oliver S., et al., 2000, *MNRAS*, 317, 55
Schwarz D. J., Starkman G. D., Huterer D., Copi C. J., 2004, *Phys. Rev. Lett.*, 93, 221301
Singal A. K., 2011, *ApJL*, 742, L23
Tiwari P., Kothari R., Naskar A., Nadkarni-Ghosh S., Jain P., 2013, *arXiv:1307.1947*
Tucci M., Martinez-Gonzalez E., Toffolatti L., Gonzalez-Nuevo J., De Zotti G., 2004, *MNRAS*, 349
Wald R. M., 1983, *Phys. Rev. D*, 28, 2118R